CRYSTAL GROWTH & DESIGN
2008
VOL. 8, NO. 6
1997–2005

Effects of Carboxylate-Modified, "Green" Inulin Biopolymers on the Crystal Growth of Calcium Oxalate

Bora Akın,[†] Mualla Öner,*[,†] Yasemin Bayram,[†] and Konstantinos D. Demadis*[,‡]

Department of Chemical Engineering, Yildiz Technical University, Davutpasa, Istanbul, 34210, Turkey, and Crystal Engineering, Growth and Design Laboratory, Department of Chemistry, University of Crete, P.O. Box 2208, Voutes Campus, Heraklion, Crete, GR71003, Greece

Received January 26, 2008

ABSTRACT: In this work, the effect of a biodegradable, environmentally friendly polysaccharide-based polycarboxylate, carboxymethyl inulin (CMI), on the crystal growth kinetics of calcium oxalate was studied at 37 °C. CMI is produced by carboxymethylation of inulin, the latter extracted from chicory roots. The spontaneous crystallization method was utilized to investigate the crystallization kinetics of calcium oxalate (CaC_2O_4, CaOx). The experimental results show that the retardation in mass transport in the growth process is controlled by the carboxylation degree of CMI and also its concentration. Our studies also indicate that polymers were effective in directing calcium oxalate crystallization from calcium oxalate monohydrate (COM) to calcium oxalate dihydrate (COD). Comparisons with the effects of polyacrylate (PAA) additive, which was also included in our experiments, show that PAA is a more effective inhibitor than CMI-15 and CMI-20, and comparable to CMI-25.

Introduction

Crystallization studies of calcium oxalate (CaC_2O_4, CaOx) have been of interest to engineers and urologists for several years.[1] Its precipitation is of particular interest to the biomineralization community[2] and also to the industrial crystallization applications' area.[3] Calcium oxalate (CaC_2O_4, CaOx) is a naturally occurring mineral found in fossils,[4] plants,[5] and mammal urinary calculi[6] and is a byproduct in some processes such as paper production,[7] food,[8] and beverage processing.[9] Plants commonly produce oxalic acid and calcium oxalate precipitates that are believed to regulate bulk free calcium within the plant.[10] In water-related industries, calcium oxalate forms scale deposits on critical industrial equipment, such as heat exchangers, boilers, and reverse osmosis membranes.[11] The problem of scale formation on heat exchangers reduces the heat transfer efficiency of the evaporation process, causing an increase in energy consumption and losses in production time.[12] Urolithiasis, the formation of urinary calculi, is one of the oldest documented diseases known to man.[13] CaC_2O_4 forms as a crystalline material in the urinary tract and is the major constituent of kidney,[14] gall,[15] and bladder stones.[16] Although normal urine is often supersaturated with respect to calcium oxalate, the formation of human kidney stones is strongly prevented by acid-rich urinary proteins[17] and naturally occurring citrate,[18] magnesium,[19] osteopontin,[20] Tamm-Horsfall protein,[21] a plethora of polycarboxylic acids,[22] copolymers of poly(acrylic acid),[23] phosphonates,[24] and even unidentified biomacromolecules.[25]

Calcium oxalate crystallization yields different hydrates, such as the thermodynamically stable monoclinic monohydrate COM ($CaC_2O_4 \cdot H_2O$, whewellite[26]), metastable tetragonal dihydrate ($CaC_2O_4 \cdot (2+x)H_2O$, $x < 0.5$, weddelite,[27]), and triclinic trihydrate ($CaC_2O_4 \cdot xH_2O$, $3 > x > 2.5$; COT[28]). COM is the thermodynamically most stable phase and has the strongest affinity for renal tubule cell membranes among the three kinds of crystals.[29] COM easily forms urinary stones because it is more difficult to eject out along with urine than COT or COD. COD is also found frequently in kidney stones,[30] plants,[31] and fossils,[32] although usually in lesser quantities. Moreover, the thermodynamically unstable trihydrate (COT) can be a precursor in CaOx stone formation.[33] Hence, an in-depth understanding of CaOx crystallization processes is essential for urologists and may augment an effort to develop effective therapeutic agents against stone formation.

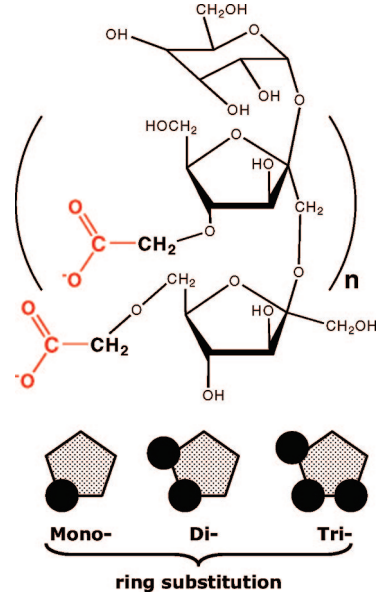

Figure 1. Schematic structure of carboxymethylinulin (CMI, carboxylate moieties are highlighted in red) and ring substitution.

The purpose of this investigation was to study the selective effect of carboxymethylinulin (CMI, Figure 1) on the crystallization kinetics and phase transformation of CaC_2O_4 using a plethora of experimental techniques (FTIR, XRD, and SEM). CMI is produced from a chemical reaction with a plant-derived biopolymer and select reagents.[34] This biopolymer, inulin,[35] is extracted from the roots of the chicory plant (dry matter content: 20–25%, inulin content: 14.9–18.3%). Inulin is a polydisperse polysaccharide consisting mainly, if not exclusively, of $\beta(2\rightarrow1)$

* Corresponding authors: E-mail: demadis@chemistry.uoc.gr; oner@yildiz.edu.tr; mualloner@gmail.com.
[†] Yildiz Technical University.
[‡] University of Crete.

10.1021/cg800092q CCC: $40.75
Published on Web 04/29/2008

fructosyl fructose units with normally, but not necessarily, one glucopyranose unit at the reducing end. It is also known that the fructose molecules are all present in the furanose form. Inulin is used as dietary fiber, a fat substitute, and a sweetener (fructose syrups). CMI has been investigated in a series of acute toxicity (oral rat, >2000 mg/kg B.W.), subacute toxicity (28 days, rat 1000 mg/kg B.W.), mutagenicity (Ames test, *in vitro* cytogenetics, no effect), and dermal sensitization studies (guinea pigs, no effect) to evaluate its toxicological profile.[36] All studies followed accepted testing guidelines as recommended by international regulatory agencies (OECD, EEC, and U.S. EPA). No significant toxicological findings were evident. Results of these toxicity studies with CMI, all conforming to internationally accepted testing standards, show that the toxicological profile of CMI is consistent with other polycarboxylates used in foods. Among other attractive attributes of CMI, its inherent biodegradability and nontoxicity are most prominent. Data that support these conclusions include toxicity (ppm) $EC_{10} > 10\,000$, bacteria (ppm) $EC_0 = 2000$, *Daphnia* (ppm) $EC_{50(24\ h)} = 5500$, and fish (ppm) $LC_0 > 10\,000$.[37] These results should be contrasted with those obtained for a polyacrylate polymer (MW = 1500) commonly used as precipitation inhibitor:[38] toxicity (ppm) $EC_{10} = 180$, bacteria (ppm) $EC_0 = 200$, *Daphnia* (ppm) $EC_{50(24\ h)} = 240$, and fish (ppm) $LC_0 = 200$.

The goal, therefore, of this research was dual: (a) to provide insights into the effects of nontoxic CMI on CaOx crystallization and inhibition efficiency and to provide a perspective for possible use of CMI in pathological stone therapy and (b) to provide a versatile and "green" inhibitor of CaOx for possible applications in the process industries. Lately, the research area of "green additives" has evolved dramatically.[39]

Experimental Section

Materials. Calcium chloride and sodium oxalate (reagent grade) were from J.T. Baker. CMI (all three grades) was from Solutia Inc., Belgium, as Dequest PB-116AB (where AB = 15 for CMI-15, AB = 20 for CMI-20, and AB = 25 for CMI-25). The number AB also indicates the degree of substitution (DS). DS is defined as the average number of carboxylate moieties per fructose unit. For example, for CMI-15, DS = 1.5; for CMI-20, DS = 2.0; for CMI-25, DS = 2.5. Carboxymethylation of inulin in laboratory scale is carried out in aqueous alkaline medium with monochloroacetic acid as the reagent (see Figure 1).[34] PAA (MW 5000) was purchased from Acros.

Crystal Growth Experiments. Crystal growth experiments were carried out in a water-jacketed Pyrex glass vessel of 1 L capacity. Supersaturated solutions for growth experiments were prepared by slow mixing of calcium chloride and sodium oxalate solutions. In experiments where additives were used a similar procedure was followed, and the freshly prepared additive solutions were normally added to the oxalate component.

The growth experiments were carried out by adding a known amount of the Ca^{2+} and oxalate stock solutions. After temperature equilibration the second component was added and pH (6.5–6.8), temperature, and calcium concentration of the reaction solutions were monitored during crystallization via personal computer equipped with appropriate software. All experiments were performed at a temperature of 37 ± 0.1 °C. In the experiments, the concentration of biopolymer was varied from 0.1 to 50 mg/L and the initial reactant ratio (RR), $[Ca^{2+}]/[C_2O_4^{2-}]$, was varied from 1/2 to 2.

The effect of polymers on the rate of precipitation of calcium oxalate was evaluated by recording the decrease of $[Ca^{2+}]$ as a function of time, in a solution containing 7.0×10^{-4} M $CaCl_2$ and $Na_2C_2O_4$ at 37 °C. The course of the reaction was followed by removing homogeneous aliquots at various times and quickly filtered through Millipore filters of 0.22 μm pore size. The aqueous phase was analyzed for $[Ca^{2+}]$ by atomic absorption spectroscopy (Perkin-Elmer AAnalyst 200). The crystals removed by filtration were examined by scanning electron microscopy (SEM), X-ray powder diffraction, and FT-IR. X-ray diffraction analyses of the crystal samples were carried out on a Phillips Panalytical X'ert Pro powder diffractometer operating with Cu Kα radiation working at 40 mA and 40 kV. The 2θ range was from 20° to 60° at scan rate of 0.020 deg $step^{-1}$. Purity of the samples was also tested by FT-IR spectral analysis. Powdered samples of precipitates (1 mg) were carefully mixed with KBr (100 mg, Merck, infrared grade) and pelletized under pressure. The pellets were analyzed using a Perkin-Elmer Spectrum One in the 4000–400 cm^{-1} region at a resolution of 4 cm^{-1}. The crystallite morphology of samples was analyzed by scanning electron microscopy (JEOL-FEG-SEM). The effect of an additive can be quantified as the ratio of the rate of crystallization of the pure solution (R_0, mg/L·min) to the rate of crystallization in the presence of additive (R_i, mg/L·min) at the same concentration and temperature. The induction period (t_{ind}) was determined by monitoring variations in $[Ca^{2+}]$, accompanied by atomic absorption spectrometric measurements. The time between the generation of a supersaturated state and the first observed change in calcium concentration was defined as t_{ind}. The time periods were determined from the recordings of the time evolution of $[Ca^{2+}]$ in solution, which is directly related to the volume of the precipitated calcium oxalate, and averaged from at least three separate experiments. Only the average values of the rate were reported. The reproducibility of this approach was ~4–5%.

Results and Discussion

Effects of CMI Biopolymers on Calcium Oxalate Crystallization. Three CMI biopolymers with an average molecular mass of ~2500 Da were investigated under identical growth conditions. CaOx crystal growth from solution begins after an initial "induction period" or "time lag" during which there is negligible change in the bulk solute concentration. The presence of minute amounts of polymers resulted in an increase in t_{ind}, followed by precipitation at a rate comparable to the rate of crystallization from pure solutions. Table 1 summarizes the results obtained with the three CMI polymers used in this study and the effect of added polymer on the crystallization rate. All polymers at 1 ppm concentration are reasonably good growth inhibitors, but CMI-25 appears to be more effective than CMI-20 and CMI-15 at the same concentration (Figure 2). CMI-25 at 1 ppm concentration can effectively block all the active growth sites and hence bring the calcium oxalate growth rate to a complete stop over a 5 h period (see Table 1).

Figure 3 shows the effect of carboxymethylation degree of the polymer on calcium oxalate inhibition. The effectiveness of biopolymers increases with increasing carboxyl content on the polymer backbone. R_0/R_i ratio increases from 15 to 74 and induction time increases from 20 to 300 min as the carboxyl content increases from 1.5 to 2.5. It was observed that products with a higher degree of carboxyl group prolong the induction period for crystallization because of the ability of the anionic carboxylate groups to adsorb on the calcium oxalate crystal surfaces. Several investigations have indicated that polymers that exhibit an inhibitory effect on crystallization kinetics of soluble salts are highly substituted with carboxyl groups.[40] Apparently the larger number of carboxylate functional groups increases the ionic attractive interactions between the adsorbate ($-COO^-$) and the positive sites (Ca^{2+}) at the solution interface. If the inhibitor ions are rapidly adsorbed, the nuclei remain subcritical and eventually disappear through dissolution. The inhibitor polyanions are then available for repeated adsorption at the edges of newly developing nuclei. This eventually leads to breakdown and disintegration of a number of the available embryos before further growth can take place. In this way outgrowth of the nuclei beyond their critical value/size is hampered. In due course, because of their thermodynamic instability, most nuclei will redissolve, thus freeing the polymer for interaction with other embryos. The polymers, by effectively reducing the number of active growth sites through adsorption on the crystal surface, will prolong induction periods.

Table 1. Effect of Polymers on Crystal Growth of CaOx at 37 °C

	CMI-15		CMI-20		CMI-25		PAA	
polymer concentration (mg/L)	R_0/R_i	induction time (min)	R_0/R_i	induction time (min)	R_0/R_i	induction time (min)	R_0/R_i	induction time (min)
				RR = 1				
0.1	1.6	0	2.6	0	3.5	2	3.4	0
0.25	3.3	0			6.1	4	11.9	34
0.5	4.9	0	13	3	18.9	6	40.6	60
1.0	14.6	20	37	50	74.1	>300	82.2	>300
5.0			50.7	>300				
10.0	19.3	100						
20.0	24.1	120						
50.0	40.1	>300						
				RR = 0.5				
1.0	1.7	0	2.1	0	2.4	0	4.6	0
10.0	3.8	0	8.6	15			6.7	16
20.0	4.1	0	24.9	25				
				RR = 2				
1.0	2.3	0	4.7	0	4.8	0	8.7	0
10.0	4.3	3	11.2	10			13.4	15
20.0	4.7	3	26.7	25				

During the induction period, most of the active growth sites are "poisoned" by the adsorbed macromolecule additives. However, some of the growth sites of lower energy may still be free to grow, and thus, the reaction proceeds at a very slow rate. The rate of precipitation/deposition of calcium oxalate following the induction period is dependent on polymer concentration. For example, the R_0/R_i ratio increases from 3.5 to 74 as the concentration of CMI-25 increases from 0.1 to 1.0 mg/L.

PAA homopolymer (MW 5000) was also evaluated as calcium oxalate inhibitor under identical experimental conditions, thus allowing a direct comparison with CMI inhibitors. Inhibition of CaOx crystallization in the presence of PAA showed that PAA is slightly more effective than any of the CMI tested here. R_0/R_i values increase from 74 to 82 in the presence of CMI-25 and PAA, respectively, at a concentration of 1 mg/L (Table 1).

The marked effect of anionic polymers on the crystal growth of calcium oxalate from supersaturated solutions has been explained in terms of the following factors: (a) Polymers may change the ionic strength of the solution; (b) polymers may form stable complexes with calcium ion; (c) adsorption of the polymer occurs on the crystal surfaces either indiscriminately or at specific growth sites; (d) polymer incorporation occurs into the calcium oxalate lattice. Under the experimental conditions employed herein, the presence of the induction period is believed to originate from inhibitor surface adsorption. The polymer concentration is too low to modify the ionic strength of the solution and the Ca^{2+} binding is sufficiently small to be ignored.[41] Polymer insertion/incorporation into the lattice can be ruled out because these macromolecules are much larger in size compared to the oxalate ion.

Since the amounts of additive in solution are small, the growth inhibition is most likely caused by biopolymer adsorption of the active growth sites on crystal surfaces rather than binding to solution Ca^{2+} ions. This assumption was tested by fitting

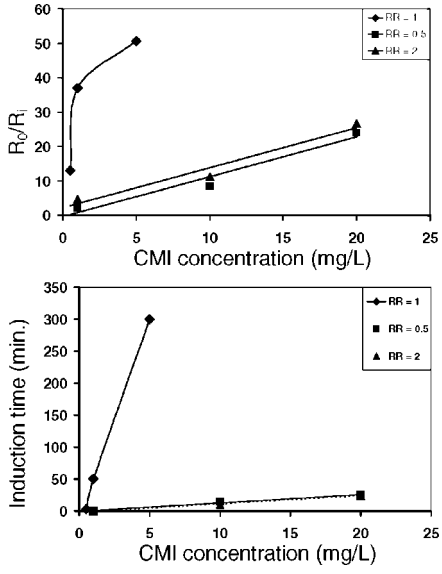

Figure 2. Effect of CMI-20 concentrations on (upper) growth rate and (lower) induction time at three different reactant ratios (RR).

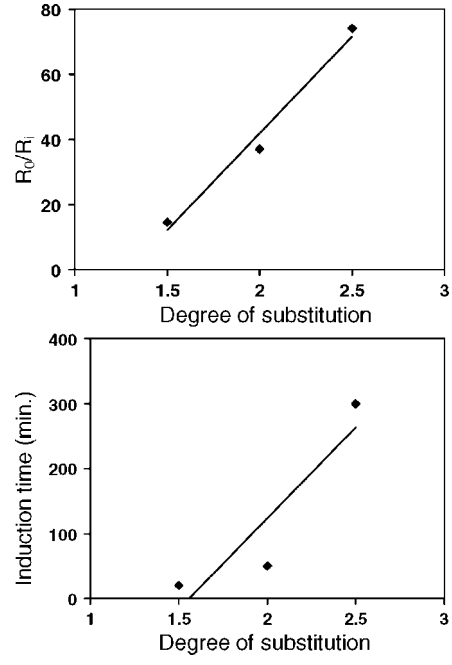

Figure 3. Effect of CMI carboxymethylation degree on (upper) growth rate and (lower) induction time (RR = 1, CMI concentration = 1.0 mg/L).

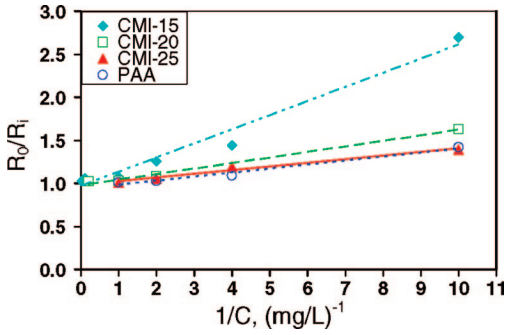

Figure 4. Langmuir-type adsorption isotherm for the effect of polymers.

the kinetic results in a Langmuir-type kinetic isotherm. When a polyelectrolyte poisons active growth sites on the crystal faces, the coverage by polymers, θ, for this adsorption model is described by eq 1.

$$\theta = KC_i/(1+KC_i) \quad (1)$$

where K is the adsorption or affinity constant, which is the ratio of the rate constants for adsorption and desorption, k_{ads}/k_{des}, and can be considered as a measure for the adsorption affinity of the polymer onto the crystal surface, and C_i is the total equilibrium concentration of the polymer. The rate in the absence of polymer, R_0, is reduced to a slower rate, R_i, according to the relationship

$$R_i = R_0(1 - \theta) \quad (2)$$

Combination of eqs 1 and 2 gives

$$\frac{R_0}{R_0 - R_i} = 1 + \frac{k_{des}}{k_{ads}}\frac{1}{C_i} \quad (3)$$

Equation 3 shows that this model predicts a linear relationship between $R_0/(R_0 - R_i)$ and $1/C_i$. The linearity of the plots of eq 3 for calcium oxalate crystal growth in the presence of polymers (Figure 4) suggests that the inhibitory effect of CMI polymers is due to adsorption at active growth sites. k_{ads}/k_{des} can be evaluated from the slope of the resulting straight line. The values of the affinity constant as calculated for PAA, CMI-25, CMI-20, and CMI-15 are 21.73, 23.86, 15.55, and 6.09 L/mg, respectively. The high value of the affinity constant for CMI-25 and PAA may reflect stronger equilibrium adsorption of PAA and CMI-25 on the crystal surface, compared to that of CMI-20 and CMI-15.

Effect of $[Ca^{2+}]/[C_2O_4^{2-}]$ Ratio on Crystal Growth Kinetics. In calcium-containing stones, COM is one of the most common constituents of the nucleus, whereas COD is formed in the outer layers.[42] The formation of the COD phase is stabilized by an excess of calcium ions. In urine the concentration of calcium may be from 5 to 30 times that of oxalate, thus favoring the higher hydrate. A series of experiments were carried out in order to investigate the influence of the calcium/oxalate molar ratio on the kinetics of crystal growth of calcium oxalate. The reactant ratio can be defined as the ratio of initial molar ratio of calcium to oxalate, $[Ca^{2+}]/[C_2O_4^{2-}]$. Typical growth curves are given in Figure 2. The faster growth rates were obtained in the presence of excess oxalate ions. R_0/R_i ratio decreased from 11.2 to 8.6 when the reactant ratio (RR) decreased from 2 to 1/2 in the presence of CMI-20 at 10 ppm. This result indicates the faster crystal growth at a reactant ratio of $[Ca^{2+}]/[C_2O_4^{2-}] = 1/2$.

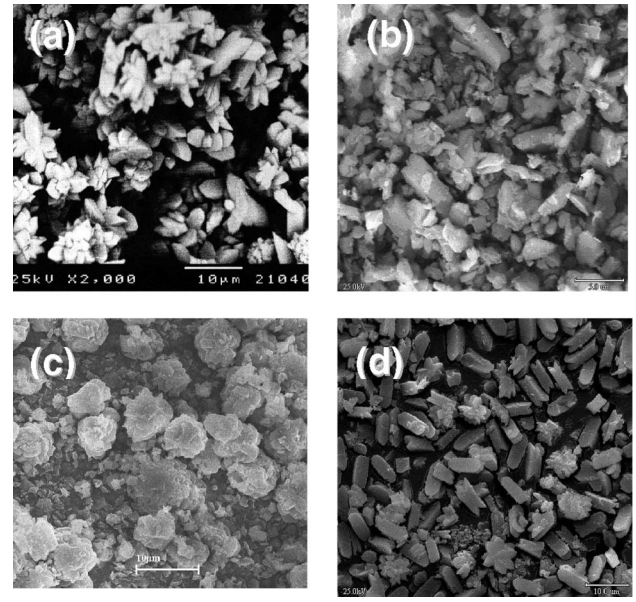

Figure 5. SEM images of CaOx crystals grown for 5 h from solution at 37 °C and reactant ratio of 1. Crystals grown from a solution containing (a) no CMI polymer, (b) 0.5 ppm CMI-15, (c) 0.5 ppm CMI-20, and (d) 0.5 ppm CMI-25.

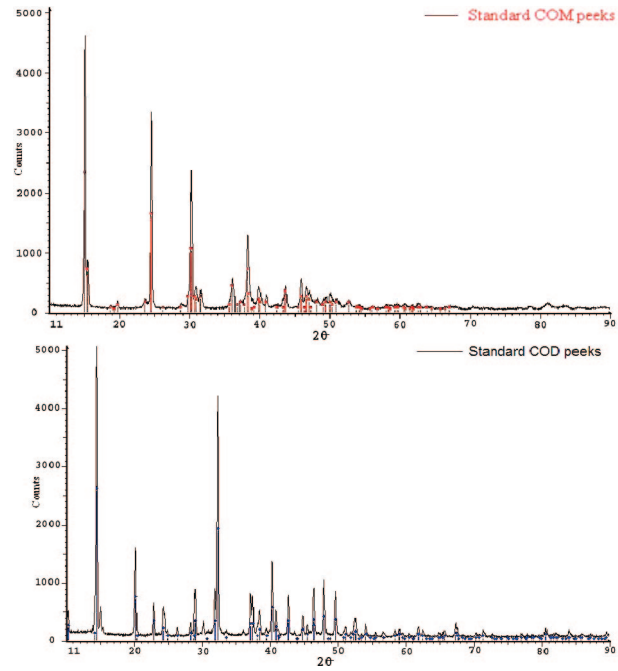

Figure 6. XRD powder patterns: (upper) no polymer additive and (lower) in the presence of CMI 20.

Effects of CMI Polymers on Calcium Oxalate Crystal Morphology. In this work, "green" carboxylate-rich biopolymers were tested for their ability to suppress growth of COM precritical nuclei and thereby favor the nucleation and growth of COD by using spontaneous crystallization experiments. The presence of polymers in supersaturated solutions affects not only the kinetics of crystal growth but crystal morphology and phase transformation of calcium oxalate crystals as well. SEM images were collected for subsequent visual analysis in order to assess the effects of CMI polymers on crystal morphology (shape and size). In all control experiments without additives, COM was the dominant phase in all concentrations (Figure 5a). The

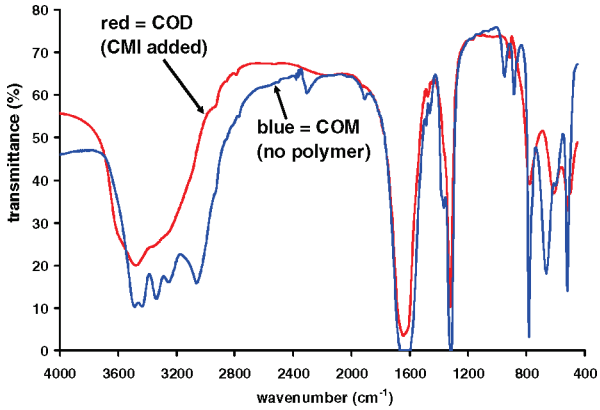

Figure 7. FT-IR spectra of calcium oxalate crystals with and without CMI-20 polymer additives.

individual crystals of platelets and a few flowerlike agglomerates were observed during crystallization of calcium oxalate in the absence of polymers. The agglomerates were about 6 μm in size. The grown prismatic crystals were identified as calcium oxalate monohydrate by XRD (Figure 6a) and compared with that of the powder diffraction.

The principal diffraction peaks of COM appear at 2θ values of 14.93° (reflection 101), at 15.29° (reflection 110), at 24.37° (reflection 020), and at 30.11° (reflection 202). FT-IR spectroscopy was utilized for further characterization of the calcium oxalate crystals (Figure 7). Spectra of all control samples showed that they consisted of COM and complemented the XRD results. The main antisymmetric carbonyl stretching band from oxalate was at 1619 cm^{-1} for COM, whereas the symmetric carbonyl stretching band was at 1317 cm^{-1}. The symmetric and asymmetric stretching bands due to the coordinated water molecules are shown as a set of five discrete peaks above 3000 cm^{-1}.

When using the polymeric additives during the crystallization, the crystal morphology and structure of calcium oxalate were modified. This modification was dependent on both biopolymer concentration and reactant ratio.

The changes in the size and morphology of the CaOx crystals as a function of polymer concentration and reactant ratio are presented in Table 2. When the polymer concentration is 0.5 ppm and the reactant ratio maintained at 1/2, 1, and 2, aggregates of monoclinic COM crystals with contact twinning are obtained in the presence of all CMI polymers (Figure 5b−d). COM is the most commonly occurring CaOx and is the thermodynamically most stable phase. It has a monoclinic structure with a space group of $P2_1/c$, and its crystal habit can best be described as a tabular single crystal.[43] However, twinning of COM crystals is common, often occurring on the large (−101) face. In this work interpenetrated twin crystals grown without additives are flattened parallel to {010} and preferentially rest on {010} faces (Figure 5d).

Addition of 1.0 ppm CMI-15 causes a distinct morphological and phase change to calcium oxalate crystals. The prismatic COM crystals (Figure 8a) totally disappeared, and as shown in Figure 8b, the product was tetragonal prisms of the COD exhibiting a prismatic habit with pyramidal endcaps with sizes of 4.2 × 3.7 μm.With an additive concentration higher than 10 mg/L, there was an outgrowth of the COD crystals along the [001] direction, resulting in elongated crystals and the development of {100} crystal faces (Figure 8c,d). The corresponding XRD pattern also confirmed that the crystal was pure COD phase, as shown in Figure 6b. The FT-IR spectrum of CaOx obtained at 1 ppm polymer solution (Figure 7) suggested the presence of COD with characteristic absorption peaks at 1643, 1327 cm^{-1} (C═O stretching) and 613 cm^{-1} (water libration). This was also evident by a loss of resolution in the 3000–3500 cm^{-1} region, i.e., a strong peak at 3462 cm^{-1} (OH stretching vibration of water) instead of five weak bands in the spectrum of COM (Figure 7). When 10 ppm PAA was present, the tetragonal COD bipyramids were considerably elongated along the *c*-axis at a reactant ratio of 2. As shown in Figure 8e the elongated rod-like prisms were an average side length of 7.3 μm and average side width of 2.3 μm.

In the case of 0.5 and 1.0 ppm concentration of CMI-20 at a reactant ratio of 1/2, agglomerated and plate-like COM crystals were crystallized, as shown in Figure 9a,b. When the concentration was increased to 10 and 20 ppm, elongated bipyramidal COD crystals were crystallized (Figure 9c,d).

Table 2. Summary of Crystallographic and Morphological Changes of CaOx at Different Reaction Conditions[a,b]

CMI-15				CMI-20				PAA			
C_i	RR	CM	average crystal Size ($a \times b \times c$) μm	C_i	RR	CM	average crystal Size ($a \times b \times c$) μm	C_i	RR	CM	average crystal Size ($a \times b \times c$) μm
1	1/2	COM	agglomerated particles	0.5	1/2	COM	contact twin and agglomerated particles	1	1/2	COD	bipyramid tetragonal prisms 4.5 × 4.2
10	1/2	COD	bipyramid tetragonal prisms 3.2 × 2.9	1	1/2	COM	agglomerated particles	10	1/2	COD	tetragonal rod-like prisms 0.5 × 0.5 × 1.8
20	1/2	COD	bipyramid tetragonal prisms 2.1 × 1.9	10	1/2	COD	tetragonal prisms 2.2 × 2 × 0.9	0.1	1	COM	platelet 4.6 × 1.0
0.5	1	COM	contact twin and agglomerated particles	20	1/2	COD	tetragonal prisms 1.9 × 1.8 × 1.2	0.5	1	COM	platelet 1.6 × 4.8
1	1	COD	bipyramid tetragonal prisms 2.4 × 2.4	0.5	1	COM	agglomerated particles	1	1	COD	tetragonal rod-like prisms 0.7 × 0.7 × 1.9
10	1	COD	bipyramid tetragonal prisms 1.7 × 1.6	1	1	COD	tetragonal prisms 1.0 × 0.9 × 0.4	10	1	COD	tetragonal rod-like prisms 0.6 × 0.6 × 2.1
20	1	COD	tetragonal prisms 1.8 × 1.6 × 0.4	1	2	COD	tetragonal prisms 2.3 × 2.1 × 1.2	10	2	COD	tetragonal rod-like prisms 2.3 × 2.3 × 7.3
0.5	2	COM	agglomerated particles	10	2	COD	tetragonal prisms 1.0 × 0.9 × 1.1				
1	2	COD	bipyramid tetragonal prisms 4.2 × 3.7	20	2	COD	tetragonal prisms 1.0 × 0.9 × 1.3				
10	2	COD	tetragonal prisms 2.5 × 2.3 × 0.8								
20	2	COD	tetragonal prisms 1.9 × 1.7 × 0.9								

[a] For bipyramid tetragonal prisms, the crystal size was represented as ($a \times b$), where a and b indicate the side length along the tetragonal axis. [b] For tetragonal prisms, the crystal size was represented as ($a \times b \times c$), where c indicates the side length perpendicular to the tetragonal axis.

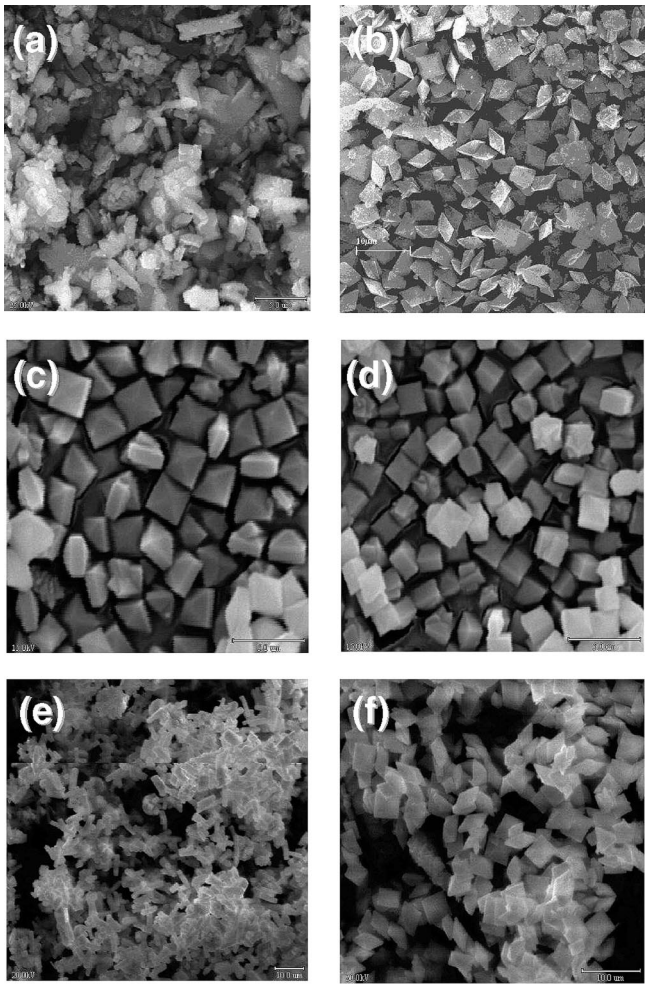

Figure 8. SEM images of CaOx crystals grown for 5 h from a solution at 37 °C and reactant ratio of 2. Crystals grown from a solution containing (a) 0.5 ppm CMI-15, (b) 1.0 ppm CMI-15, (c) 10 ppm CMI-15, (d) 20 ppm CMI-15, (e) 10 ppm PAA, and (f) 1 ppm PAA at a RR of 1/2.

The dimensions of a minimum of 30 crystals in each sample were measured from SEM photomicrographs. The average value of the dimensions is given in Table 2. It can be seen that the side length perpendicular to the tetragonal axis increases with increasing polymer concentration. As polymer concentration increases, COD morphology varies from the form of a tetragonal bipyramid dominated with (101) faces to the form of a tetragonal prism dominated with (100) faces. The same behavior was observed with PAA. In the presence of 1 ppm PAA, tetragonal bipyramidal crystals were obtained at a reactant ratio of 1/2. The square prisms were 4.5 μm in side length and 4.2 in side width (see Figure 8f). When 10 ppm PAA was present, a distinct morphological and phase change of calcium oxalate crystals occurred. It can be observed that the square prisms were considerably elongated along the *c*-axis (see Table 2). The change of crystal habit of COD caused by added polymer is schematically shown in Figure 10. In a previous study, it was reported that a block copolymer (poly(ethyleneglycol)-*block*-poly(methacrylic acid)) preferentially induces crystallization of rod-like tetragonal prisms dominated by the (100) faces.[44]

COD has a tetragonal structure with a space group of *I*4/*m* and a crystal habit that can be best described as tetragonal bipyramidal.[45] The calcium surface concentration of the COD on the (100) face (0.0439 ions/A^2) is greater than that on the (101) face (0.0225 ions/A^2). This result implies that the (100) face can adsorb a higher number of carboxylate moieties from the polymers. Therefore the interactions between polymer and the COD (100) faces resulted in a gradual morphological transition of COD crystals from tetragonal bipyramids to elongated tetragonal prisms with increasing polymer concentration.

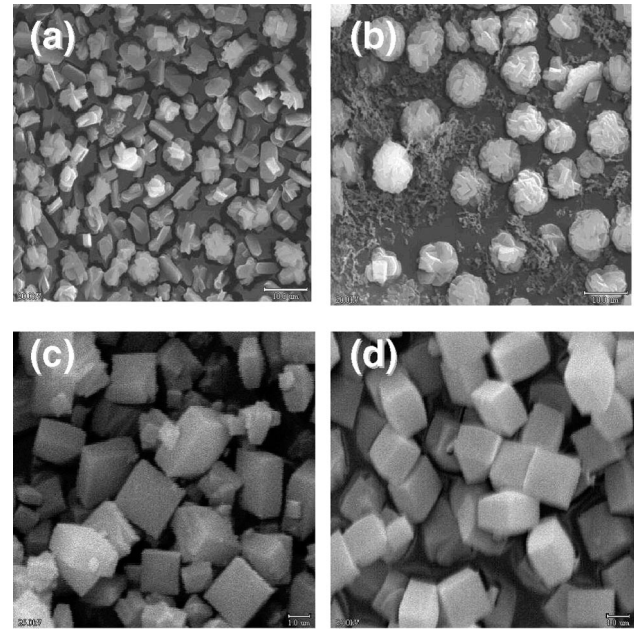

Figure 9. SEM images of CaOx crystals grown for 5 h from a solution at 37 °C and reactant ratio 1/2. Crystals grown from a solution containing (a) 0.5 ppm CMI-20, (b) 1 ppm CMI-20, (c) 10 ppm CMI-20, and (d) 20 ppm CMI-20.

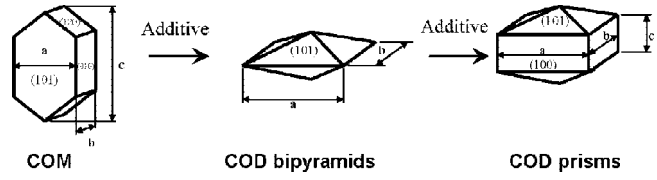

Figure 10. Schematic representation of the morphological influence of biopolymer on CaOx crystals.

A large number of reports have appeared in the literature on the effects of various additives on calcium oxalate crystallization. These include glutamic and aspartic acids,[46a,d] polyphosphate,[46] sodium dodecyl sulfate,[46] polyethyleneglycol,[46] sodium cholate,[46] maleic acid copolymers,[47] polyaspartic and polyglutamic acids,[48] poly(styrene-*alt*-maleic acid),[49] various polyhydroxycarboxylic acids,[50] acrylic polymers,[51] tartarates,[52] diisooctyl sulfosuccinate,[53] mucin,[54] chondroitin sulfates,[55] Tamm-Horsfall proteins,[56] herbal extracts,[57] uric acid,[58] poly(sodium 4-styrenesulfonate),[59] liposome solutions of different carboxylates,[60] polypeptides,[30] fluorescent molecules,[61] algae-derived, sulfated polysaccharides,[62] osteopontin,[63] aspartic-rich synthetic peptides,[64] synthetic osteopontin phosphopeptides,[65] uropontin,[66] pyrophosphate,[67] citrate and isocitrate,[68] tryptophan,[69] dipalmitoylphosphatidylcholine,[70] inositol hexaphosphate (phytate),[71] glycosaminoglycans,[72] fibronectin,[73] glycoproteins,[74] unidentified macromolecules from whole human urine,[75] α-ketoglutaric acid,[76] adenosine phosphates,[77] various aminoacids,[78] and poly(ethyleneglycol-*block*-acrylic acid) polymers.[23]

A number of important observations point to the way carboxylate-containing macromolecules may affect CaOx crystallization. Elegant work by Ward et al. (with AFM)[48c–e,63b] and by Kim et al. (with SEM and XRD)[48f] has focused on studying

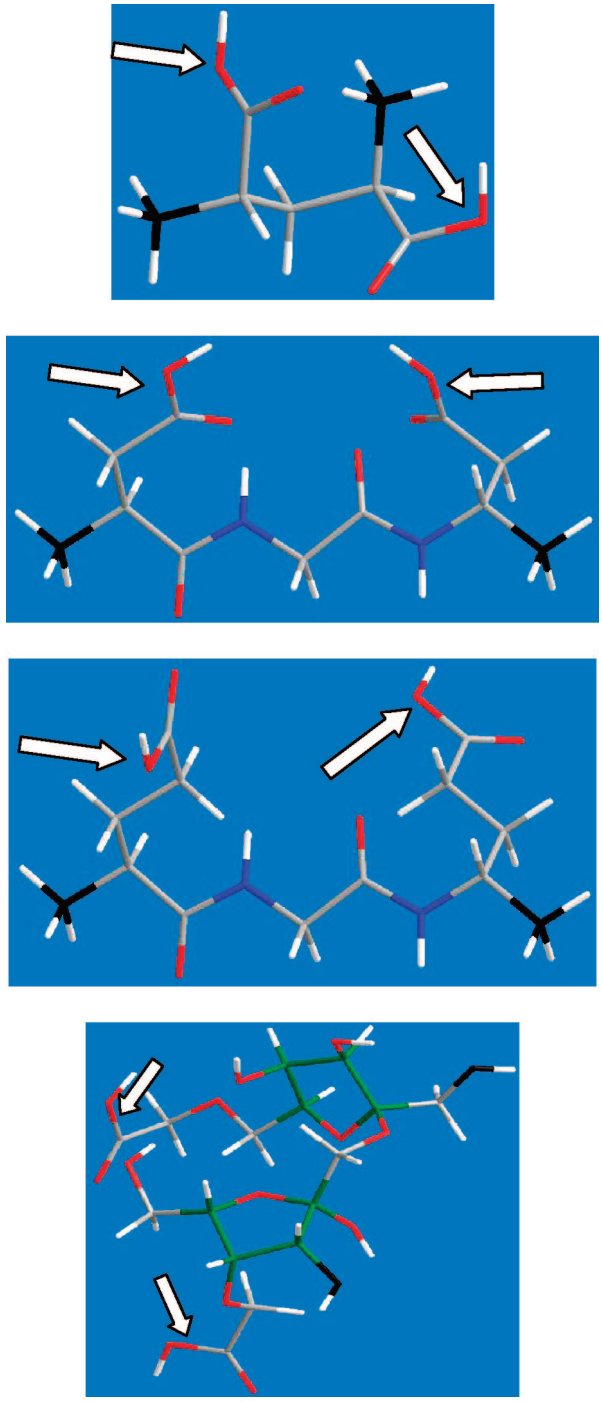

Figure 11. Energy-minimized fragments of the polymers polyacrylate, polyaspartate, polyglutamate, and CMI. Color codes: gray C; white H; red O; blue N. The atoms that link these fragments with the remaining polymer are colored in black. For clarity, carbon atoms in the CMI rings are colored green. Carboxylate moieties that interact with Ca^{2+} on the CaOx crystal surfaces are indicated by arrows.

the interactions of polymers with pendant carboxylate groups (polyacrylate, polyaspartate, and polyglutamate; see Figure 11) with various crystallographic planes of the CaOx monohydrate crystals. These studies revealed the importance of cooperative binding of the polymer carboxylate groups to Ca^{2+} sites on the crystal surfaces of the "steps". Specifically, when growth of the (001) and (021) hillocks was studied, it was documented that the ranking of polymeric inhibitors was polyacrylate > polyaspartate > polyglutamate. Polyacrylate was also a potent inhibitor of growth on the (021) and (12$\bar{1}$) planes. Data also revealed that polyglutamate was more effective than polyaspartate for both (021) and (12$\bar{1}$) planes. However, polyaspartate was more effective than polyglutamate in inhibiting the growth of (010) hillocks. Overall, the binding behavior of carboxylate-containing macromolecules to several crystal faces is clearly complex.

Another interesting theme to be examined is the negative "charge density", or, in other words, the number of bonds separating the negative charge located on the carboxylate groups. Bonds separating the deprotonated oxygen in the $-COO^-$ groups in the polymers' backbone are polyacrylate 6, polyaspartate 12, polyglutamate 14, CMI-16 (for CMI-15, containing one carboxylate group per D-fructofuranose ring), or CMI-7 (for CMI-20, containing two carboxylate groups on the same D-fructofuranose ring), or CMI-14 (for CMI-20, containing two carboxylate groups on neighboring D-fructofuranose rings); see Figure 11. On the basis of the work of Ward et al., there is an inversely proportional relationship between inhibitory activity and the number of bonds separating the carboxylate units. Our results confirm this significant observation, as the inhibitory activity ranking is CMI-15 < CMI-20 < CMI-25 ~ PAA. The effects of charge density on inhibitory activity may be a wider theme in inhibition chemistry. A recent report on the inhibitory activity of a series of polyamines on silica formation demonstrated that as the proximity of the $-NH_3^+$ groups increases (note that for effective silica inhibition a cationic charge is necessary) on the polymer backbone, inhibitory activity increases as well.[79]

Conclusions

Biopolymers tested in this study are effective as growth inhibitors of CaOx under the described experimental conditions. The higher affinity of CMI-25 for CaOx crystal surfaces is reflected in the more profound effect of CMI-25 on the CaOx crystal growth rate. CMI-25 polymeric chains have a higher anionic charge density because they contain a higher number of carboxyl groups compared to CMI-15 or CMI-20. Therefore, they mitigate the interaction ability of the appended anionic $-COO^-$ groups with the solid phase. The polymer backbone can then act as a "fence" on the crystal surface, thus forming an obstacle for propagating steps that lead to further crystal growth. The results described herein indicate that anionic biopolymers can inhibit calcium oxalate crystal growth and that such inhibition is directly linked to fractional coverage of adsorption sites. The degree of inhibition of calcium oxalate crystallization by CMI biopolymers is related to the maximum surface charge density due to adsorbed polymer.

The polymer concentration and the $[Ca^{2+}]/[C_2O_4^{2-}]$ ratio are found to be important parameters for the control of morphologies and phase transformation of CaOx crystals. Agglomerated and twinned COM crystals formed in control experiments. The presence of CMI polymers favors the transition of COM to COD crystals. The high binding affinity of the CMI polymer molecules resulted in morphological transition of COD crystals from tetragonal bipyramids dominated by the (101) faces to elongated tetragonal prisms dominated by the (100) faces. CMI-25 was found to be a comparable inhibitor to the previously studied PAA.

Acknowledgment. M.Ö. thanks the Scientific and Technological Research Council of Turkey (TUBİTAK, Project No: 105M329), and K.D.D. thanks the General Secretariat of Science and Technology (Greece, under contract #GSRT 2007-202e)

for funding this work under a Bilateral Cooperation Program between Turkey and Greece.

References

(1) (a) Ajayi, L.; Jaeger, P.; Robertson, W.; Unwin, R. *Medicine* **2007**, *35*, 415–419. (b) Dent, C. E.; Sutor, D. J. *Lancet* **1971**, *298*, 775–778. (c) Webber, D.; Rodgers, A. L.; Sturrock, E. D. *J. Cryst. Growth* **2003**, *259*, 179–189.

(2) (a) Hesse, A.; Tiselius, H.-G.; Jahnen, A. *Urinary Stones: Diagnosis, Treatment and Prevention of Recurrence*, 2nd ed.; Karger: Switzerland, 2002. (b) Sikiric, M. D.; Furedi-Milhofer, H. *Adv. Colloid Interface Sci.* **2006**, *128–130*, 135–158.

(3) (a) Doherty, W. O. S. *Ind. Eng. Chem. Res.* **2006**, *45*, 642–647. (b) Yu, H.; Sheikholeslami, R.; Doherty, W. O. S. *Powder Technol.* **2005**, *160*, 2–6.

(4) Franceschi, V. R.; Horner, H. T. *Bot. Rev.* **1980**, *46*, 361–427.

(5) (a) Pennisi, S. V.; McConnell, D. B.; Gower, L. B.; Kane, M. E.; Lucansky, T. *New Phytol.* **2001**, *150*, 111–120. (b) Wadsten, T.; Moberg, R. *Lichenologist* **1985**, *17*, 239–245.

(6) Nakagawa, Y.; Abram, V.; Coe, F. L. *Am. J. Physiol.* **1984**, *247*, F765–F772.

(7) (a) Ulmgren, P.; Rådeström, R. *Nordic Pulp Paper Res. J.* **2001**, *16*, 389. (b) Reeve, D. W.; Weishar, K M. *Tappi J.* **1991**, *74*, 164. (c) Potter, S.; Reath, S.; Hussein, A.; Gee, W.; Lawrence, V.; Drummond, *J. Wood Sci. Technol.* **2003**, *37*, 321–329.

(8) Perera, C. O.; Hallett, I. C.; Nguyen, T. T.; Charles, J. C. *J. Food Sci.* **1990**, *55*, 1066–1069.

(9) Masár, M.; Zuborová, M.; Kaniansky, D.; Stanislawski, B. *J. Sep. Sci.* **2003**, *26*, 647–652.

(10) Franceschi, V. R.; Nakata, P. A. *Ann. Rev. Plant Biol.* **2005**, *56*, 41–71.

(11) Yu, H.; Sheikholeslami, R.; Doherty, W. O. S. *J. Cryst. Growth* **2004**, *265*, 592–603.

(12) Demadis, K. D. In *Compact Heat Exchangers and Enhancement Technology for the Process Industries*; Shah, R. K., Ed.; Begell House Inc.: New York, 2003; pp 483–490.

(13) Grases, F.; Söhnel, F.; Garcia-Ferragut, L.; Costa-Bauza, A. *Scand. J. Urol. Nephrol.* **1995**, *29*, 421–428.

(14) (a) Schwarz, R. D.; Dwyer, N. T. *Urology* **2006**, *67*, 812–816. (b) Asplin, J. R.; Coe, F. L. *J. Urol.* **2007**, *177*, 565–569.

(15) Schoenfield, L. J.; Marks, J. W. *Am. J. Surg.* **1993**, *165*, 427–430.

(16) *Pathogenic Basis of Disease*, 6th ed.; Robbins, S. L., Cortran, R. S., Kumar, V., Collins, T., Eds.; Harcourt Asia PTE Ltd.: Singapore, 1999.

(17) (a) Garti, N.; Tibika, F.; Sarig, S.; Perlberg, S. *Biochem. Biophys. Res. Commun.* **1980**, *97*, 1154–1162. (b) Basavaraj, D. R.; Biyani, C. S.; Browning, A. J.; Cartledge, J. J. *EAU-EBU Update Ser.* **2007**, *5*, 126–136.

(18) (a) Weaver, M. L.; Qiu, S. R.; Hoyer, J. R.; Casey, W. H.; Nancollas, G. H.; De Yoreo, J. J. *J. Cryst. Growth* **2007**, *306*, 135–145. (b) Sidhu, H.; Gupta, R.; Thind, S. K.; Nath, R. *Urol. Res.* **1986**, *14*, 299–303. (c) Bek-Jensen, H.; Fornander, A.-M.; Nilsson, M.-A.; Tiselius, H. -G. *Urol. Res.* **1996**, *24*, 67–71. (d) Qiu, S. R.; Wierzbicki, A.; Salter, E. A.; Zepeda, S.; Orme, C. A.; Hoyer, J. R.; Nancollas, G. H.; Cody, A. M.; De Yoreo, J. J. *J. Am. Chem. Soc.* **2005**, *127*, 9036–9044.

(19) Wunderlich, W. *Urol. Res.* **1981**, *9*, 157–161.

(20) (a) Wang, L.; Zhang, W.; Qiu, S. R.; Zachowicz, W. J.; Guan, X.; Tang, R.; Hoyer, J. R.; De Yoreo, J. J.; Nancollas, G. H. *J. Cryst. Growth* **2006**, *291*, 160–165. (b) Konya, E.; Umekawa, T.; Iguchi, M.; Kurita, T. *Eur. Urol.* **2003**, *43*, 564–571.

(21) (a) Gokhale, J. A.; Glenton, P. A.; Khan, S. R. *J. Urol.* **2001**, *166*, 1492–1497. (b) Ganter, K.; Bongartz, B.; Hesse, A. *Urology* **1999**, *53*, 492–495.

(22) (a) Cody, A. M.; Cody, R. D. *J. Cryst. Growth* **1994**, *135*, 235–245. (b) Azoury, R.; Randolph, A. D.; Drach, G. W.; Perlberg, S.; Garti, N.; Sarig, S. *J. Cryst. Growth* **1983**, *64*, 389–392. (c) Ouyang, J.-M. *Mater. Sci. Eng., C* **2006**, *26*, 679–682.

(23) (a) Akyol, E.; Bozkurt, A.; Öner, M. *Polym. Adv. Technol.* **2006**, *17*, 58–65. (c) Akyol, E.; Öner, M. *J. Cryst. Growth* **2007**, *307*, 137–144.

(24) Meyer, J. L.; Lee, K. E.; Bergert, J. H. *Calc. Tiss. Res.* **1977**, *28*, 83–86.

(25) Sorensen, S.; Hansen, K.; Bak, S.; Justesen, S. J. *Urol. Res.* **1990**, *18*, 373–379.

(26) Ogbuji, L. U.; Batich, C. D. *J. Ultrastruct. Res.* **1985**, *90*, 1–8.

(27) Kaloustian, J.; El-Moselhy, T. F.; Portugal, T. F. *Clin. Chim. Acta* **2003**, *334*, 117–129.

(28) Opalko, F. J.; Adair, J. H.; Khan, S. R. *J. Cryst. Growth* **1997**, *181*, 410–417.

(29) Rabinovich, Y. I.; Esayanur, M.; Daosukho, S.; Byer, K. J.; El-Shall, H. E.; Khan, S. R. *J. Colloid Interface Sci.* **2006**, *300*, 131–140.

(30) Wesson, J. A.; Worcester, E. M.; Kleinman, J. G. *J. Urol.* **2000**, *163*, 1343–1348.

(31) Joshi, V. S.; Parekh, B. B.; Joshi, M. J.; Vaidya, A. B. *J. Cryst. Growth* **2005**, *275*, e1403–e1408.

(32) Li, X.; Zhang, D.; Lynch-Holm, V. J.; Okita, T. W.; Franceschi, V. *Plant Physiol.* **2003**, *133*, 549–559.

(33) Heijnen, W. M. M. *J. Cryst. Growth* **1982**, *57*, 216–232.

(34) Verraest, D. L.; Peters, J. A.; Batelaan, J. G.; van Bekkum, H. *Carbohydr. Res.* **1995**, *271*, 101–112.

(35) (a) Stevens, C. V.; Meriggi, A.; Booten, K. *Biomacromolecules* **2001**, *2*, 1–16. (b) Johnson, L.; Verraest, D. L.; Besemer, A. C.; van Bekkum, H.; Peters, J. A. *Inorg. Chem.* **1996**, *35*, 5703–5710. (c) Niness, K. R. *J. Nutr.* **1999**, *129*, 1402S–1406S. (d) Won, C.-Y.; Chu, C.-C. *J. Appl. Polym. Sci.* **1999**, *70*, 953–963. (e) Verraest, D. L.; Peters, J. A.; Kuzee, H. C.; Raaijmakers, H. W. C.; van Bekkum, H. *Carbohydr. Polym.* **1998**, *37*, 209–214. (f) Stevens, C. V.; Meriggi, A.; Peristeropoulou, M.; Christov, P. P.; Booten, K.; Levecke, B.; Vandamme, A.; Pittevils, N.; Tadros, T. F. *Biomacromolecules* **2001**, *2*, 1256–1259. (g) Andre, I.; Putaux, J. L.; Chanzy, H.; Taravel, F. R.; Timmermans, J. W.; de Wit, D. *Int. J. Biol. Macromol.* **1996**, *18*, 195–204.

(36) Johannsen, F. R. *Food Chem. Toxicol.* **2003**, *41*, 49–59.

(37) Data were kindly provided from Solutia Inc.

(38) (a) Mishra, S.; Patil, A. D. *Chem. Eng. Technol.* **2002**, *25*, 573–577. (b) van der Leeden, M. C.; Rosmalen, G. M. *J. Colloid Interface Sci.* **1995**, *171*, 142–149.

(39) (a) Anastas, P. T.; Warner, J. C. *Green Chemistry: Theory and Practice*; Oxford University Press: New York, 1998. (b) Useful information on green chemistry can be found in the U.S. Environmental Protection Agency web page at http://www.epa.gov/greenchemistry (accessed April 1, 2008). (c) Several principles of green chemistry are analyzed in the Canadian Green Chemistry Network, at http://www.greenchemistry.ca (accessed April 1, 2008). (d) Demadis, K. D.; Neofotistou, E.; Mavredaki, E.; Tsiknakis, M.; Sarigiannidou, E.-M.; Katarachia, S. D. *Desalination* **2005**, *179*, 281–295. (e) Demadis, K. D.; Mavredaki, E. *Env. Chem. Lett.* **2005**, *3*, 127–131. (f) Verraest, D. L.; Peters, J. A.; van Bekkum, H.; van Rosmalen, G. M. *J. Am. Oil Chem. Soc.* **1996**, *73*, 55–60.

(40) (a) Öner, M.; Norwig, J.; Meyer, W. H.; Wegner, G. *Chem. Mater.* **1998**, *10*, 460–463. (b) Doherty, W. O. S.; Fellows, C. M.; Gorjian, S.; Senogles, E.; Cheung, W. H. *J. Appl. Polym. Sci.* **2004**, *91*, 2035–2041. (c) Lioliou, M. G.; Paraskeva, C. A.; Koutsoukos, P. G.; Payatakes, A. C. *J. Colloid Interface Sci.* **2006**, *303*, 164–170.

(41) Ca^{2+} binding by CMI (expressed in mmol Ca^{2+}/g CMI) was determined, and the following results were obtained: at pH 5.0, 0.15 (CMI-15), 0.25 (CMI-20), 0.30 (CMI-25); for pH 5.5, 0.50 (CMI-15), 0.70 (CMI-20), 0.90 (CMI-25); for pH 6.0, 0.60 (CMI-15), 1.00 (CMI-20), 1.30 (CMI-25); for pH 8.0: 0.75 (CMI-15), 1.20 (CMI-20), 1.40 (CMI-25); for pH 10.0, 0.80 (CMI-15), 1.30 (CMI-20), 1.70 (CMI-25).

(42) Sheehan, M. E. The Kinetics of Crystal Growth of Calcium Oxalate. Ph.D. Thesis, State University of New York at Buffalo, 1981.

(43) (a) Tazzoli, V.; Domeneghetti, C. *Am. Mineral.* **1980**, *65*, 327. (b) Lepage, L.; Tawashi, R. *J. Pharm. Sci.* **1982**, *71*, 1059–1062.

(44) Zhang, D.; Qi, L.; Ma, J.; Cheng, H. *Chem. Mater.* **2002**, *14*, 2450–2457.

(45) Sterling, C. *Acta Crystallogr.* **1965**, *18*, 917–921.

(46) (a) Furedi-Milhofer, H.; Sikiric, M.; Tunik, L.; Filipovic-Vincekovic, N.; Garti, N. *Int. J. Mod. Phys. B* **2002**, *16*, 359–366. (b) Skrtic, D.; Filipovic-Vincekovic, N.; Babic-Ivancic, V.; Tusek-Bozic, L. *J. Cryst. Growth* **1993**, *133*, 189–195. (c) Shirane, Y.; Kagawa, S. *J. Urol.* **1993**, *150*, 1980–1983. (d) Orme, C. A.; Noy, A.; Wierzbicki, A.; McBride, M. T.; Grantham, M.; Teng, H. H.; Dove, P. M.; DeYoreo, J. J. *Nature* **2001**, *411*, 775–779.

(47) Bouropoulos, K.; Bouropoulos, N.; Melekos, M.; Koutsoukos, P. G.; Chitanu, G. C.; Anghelescu-Dogaru, A. G.; Carpov, A. A. *J. Urol.* **1998**, *159*, 1755–1761.

(48) (a) Campbell, A. A.; Ebrahimpour, A.; Perez, L.; Smesko, S. A.; Nancollas, G. H. *Calcif. Tissue Int.* **1989**, *45*, 122–128. (b) Wesson, J. A.; Worcester, E. *Scanning Microsc.* **1996**, *10*, 415–424. (c) Jung, T.; Sheng, X.; Choi, C. K.; Kim, W.-S.; Wesson, J. A.; Ward, M. D. *Langmuir* **2004**, *20*, 8587–8596. (d) Guo, S.; Ward, M. D.; Wesson, J. A. *Langmuir* **2002**, *18*, 4284–4291. (e) Sheng, X.; Ward, M. D.; Wesson, J. A. *J. Am. Chem. Soc.* **2003**, *125*, 2854−2855. (f) Jung, T.; Kim, W.-S.; Choi, C. K. *J. Cryst. Growth* **2005**, *279*, 154–162.

(49) Yu, J.; Tang, H.; Cheng, B.; Zhao, X. *J. Solid State Chem.* **2004**, *177*, 3368–3374.

(50) Grases, F.; Millan, A.; Garcia-Raso, A. *J. Cryst. Growth* **1988**, *89*, 496–500.
(51) Öner, M.; Calvert, P. *Mater. Sci. Eng. C* **1994**, *2*, 93–101.
(52) Ouyang, J.-M.; Deng, S.-P.; Zhou, N.; Tieke, B. *Colloid Surf. A* **2005**, *256*, 21–27.
(53) Tunik, L.; Furedi-Milhofer, H.; Garti, N. *Langmuir* **1998**, *14*, 3351–3355.
(54) Akbarieh, M.; Tawashi, R. *Scanning Microsc.* **1991**, *5*, 1019–1027.
(55) Kim, K. M. *Scanning Microsc.* **1996**, *10*, 445–457.
(56) Deganello, S.; Campbell, A. A.; Robertson, W. G.; Fairing, J. D. *Scanning Microsc.* **1993**, *7*, 1111–1118.
(57) Joshi, V. S.; Parekh, B. B.; Joshi, M. J.; Vaidya, A. B. *J. Cryst. Growth* **2005**, *275*, e1403–e1408.
(58) Frincu, M. C.; Fogarty, C. E.; Swift, J. A. *Langmuir* **2004**, *20*, 6524–6529.
(59) Yu, J.; Tang, H.; Cheng, B. *J. Colloid Interface Sci.* **2005**, *288*, 407–411.
(60) Ouyang, J.-M.; Duan, L.; He, J.-H.; Tieke, B. *Chem. Lett.* **2003**, *32*, 268–269.
(61) Touryan, L. A.; Clark, R. H.; Gurney, R. W.; Stayton, P. S.; Kahr, B.; Vogel, V. *J. Cryst. Growth* **2001**, *233*, 380–388.
(62) Wu, X. M.; Ouyang, J. M.; Deng, S. P.; Cen, Y. Z. *Chin. Chem. Lett.* **2006**, *17*, 97–100.
(63) (a) Taller, A.; Grohe, B.; Rogers, K. A.; Goldberg, H. A.; Hunter, G. K. *Biophys. J.* **2007**, *93*, 1768–1777. (b) Sheng, X.; Jung, T.; Wesson, J. A.; Ward, M. D. *Proc. Natl. Acad. Sci.* **2005**, *102*, 267–272. (c) Qiu, S. R.; Wierzbicki, A.; Orme, C. A.; Cody, A. M.; Hoyer, J. R.; Nancollas, G. H.; Zepeda, S.; DeYoreo, J. J. *Proc. Natl. Acad. Sci.* **2004**, *101*, 1811–1815. (d) Sorensen, S.; Justesen, S. J.; Johnsen, A. H. *Urol. Res.* **1995**, *23*, 327–334.
(64) Wang, L.; Qiu, S. R.; Zachowicz, W.; Guan, X.; DeYoreo, J. J.; Nancollas, G. H.; Hoyer, J. R. *Langmuir* **2006**, *22*, 7279–7285.
(65) Grohe, B.; O'Young, J.; Ionescu, D. A.; Lajoie, G.; Rogers, K. A.; Karttunen, M.; Goldberg, H. A.; Hunter, G. K. *J. Am. Chem. Soc.* **2007**, *129*, 14946–14951.
(66) Shiraga, H.; Min, W.; VanDusen, W. J.; Clayman, M. D.; Miner, D.; Terrell, C. H.; Sherbotie, J. R.; Foreman, J. W.; Przysiecki, C.; Neilson, E. G.; Hoyer, J. R. *Proc. Natl. Acad. Sci.* **1992**, *89*, 426–430.
(67) Ryall, R. L.; Hibberd, C. M.; Marshall, V. R. *Urol. Res.* **1985**, *13*, 285–289.
(68) (a) Baumann, J. M.; Wacker, M. *Urol. Res.* **1979**, *7*, 183–188. (b) Hennequin, C.; Lalanne, V.; Daudon, M.; Lacour, B.; Drueke, T. *Urol. Res.* **1993**, *21*, 101–108.
(69) Shen, Y.; Li, S.; Xie, A.; Xu, W.; Qiu, L.; Yao, H.; Yu, X.; Chen, Z. *Colloid Surf. B* **2007**, *58*, 298–304.
(70) Deng, S.-P.; Ouyang, J.-M. *Coll. Surf. A* **2005**, *257–258*, 47–50.
(71) Saw, N. K.; Chow, K.; Rao, P. N.; Kavanagh, J. P. *J. Urol.* **2007**, *177*, 2366–2370.
(72) Gohel, M. D. I.; Shum, D. K. Y.; Tan, P. C. *Carbohydr. Res.* **2007**, *342*, 79–86.
(73) Tsujihata, M.; Miyake, O.; Yoshimura, K.; Kakimoto, K.-I.; Takahara, S.; Okuyama, A. *J. Urol.* **2000**, *164*, 1718–1723.
(74) (a) Atmani, F.; Lacour, B.; Drueke, T.; Daudon, M. *Urol. Res.* **1993**, *21*, 61–66. (b) Umekawa, T.; Iguchi, M.; Konya, E.; Yamate, T.; Amasaki, N.; Kurita, T. *Urol. Res* **1999**, *27*, 315–318.
(75) (a) Edyvane, K. A.; Hibberd, C. M.; Harnett, R. M.; Marshall, V. R.; Ryall, R. L. *Clin. Chim. Acta* **1987**, *161*, 329–338. (b) Miyake, O.; Kakimoto, K.; Tsujihata, M.; Yoshimura, K.; Takahara, S.; Okuyama, A. *Urology* **2001**, *58*, 493–497.
(76) Atanassova, S.; Neykov, K.; Gutzow, I. *J. Cryst. Growth* **1996**, *160*, 148–153.
(77) Grases, F.; March, J. G.; Costa-Bauza, A. *J. Colloid Interface Sci.* **1989**, *128*, 382–387.
(78) Brecevic, J.; Kralj, D. *J. Cryst. Growth* **1986**, *79*, 178–184.
(79) Demadis, K. D.; Stathoulopoulou, A. *Ind. Eng. Chem. Res.* **2006**, *45*, 4436–4440.

CG800092Q